GEOPHYSICS, VOL. 71, NO. 3 (MAY-JUNE 2006); P. S85–S97, 6 FIGS.
10.1190/1.2192914

Highly accurate absorbing boundary conditions for wide-angle wave equations

A. Homayoun Heidari[1] and Murthy N. Guddati[2]

ABSTRACT

We develop a new class of absorbing boundary conditions (ABCs) to prevent unwanted artifacts and wraparounds associated with aperture truncation in migration/modeling using high-order, one-way wave equations. The fundamental approach behind the proposed development is the efficient discretization of the half-space, beyond the boundary of interest, using midpoint-integrated imaginary finite elements, an idea recently utilized in the development of effective one-way wave equations. The proposed absorbing boundary conditions essentially add absorbing layers at the aperture truncation points. We derive the absorbing boundary conditions, analyze their properties, and develop a stable explicit finite-difference scheme to solve the downward-continuation problem modified by these boundary conditions. With the help of numerical examples, we conclude that with as few as three absorbing layers, i.e., two additional gridpoints, the waves can be absorbed completely, thus preventing associated artifacts.

INTRODUCTION

The numerical solution of wave propagation for modeling and migration must be carried out in a truncated domain because of the limitations of survey aperture and computation costs. Once the domain is truncated, the absorbing boundary conditions (ABCs) should be used at the artificial boundaries to prevent wraparounds in modeling and unwanted artifacts in migration. ABCs for full wave equations have been under investigation since the 1970s, and many successful methods have been developed in this context. Most of the existing ABCs can be classified into two categories: differential equation based and material based (Shlager and Schneider, 1995). Differential-equation-based methods are formulated by factoring the governing equation at the boundary and allowing only outgoing waves, a familiar method used in deriving one-way wave equations (OWWEs) for migration. Differential-equation-based ABCs can be further classified into local and nonlocal ABCs. Nonlocal ABCs are based on Green's function of the half-space (exact impedance) and are highly accurate but tend to be very expensive and unsuitable for large-scale problems. On the other hand, local ABCs approximate the impedance but are computationally efficient. Local ABCs were pioneered by Lindman (1975) and Engquist and Majda (1977, 1979), who proposed a series of highly accurate ABCs that have been implemented only recently [see Givoli (2004) for survey]. Examples of other early works on local ABCs are Clayton and Engquist (1977), Raynolds (1978), and Keys (1985).

In contrast with the differential-equation-based ABCs, material-based ABCs are modeled by surrounding the computational domain with a lossy material to dampen the outgoing waves and reduce the artificial reflection from the boundaries. The most robust application of this approach is the method of perfectly matched layers (PML), introduced by Berenger (1994) and later interpreted and enhanced by several other researchers [e.g., Chew et al. (1997) and Sacks et al. (1995)]. Despite the conceptual difference between the material-based and local ABCs, Asvadurov et al. (2003) show a mathematical link between the two, which is further simplified by Guddati and Lim (2004), who illustrate the superior performance of local ABCs over the conventional PML method.

The ABCs may be used with slight modification for reverse-time migration, as it is performed using the adjoint of the full wave equation. However, wave equation-based migration is mostly performed using OWWEs (Berkhout 1985; Claerbout, 1985; Gardner, 1985; Stolt and Benson, 1986). Hence, ABCs developed for the full wave equation cannot be used for such migration. This is because the ABC formulation must be consistent with, and devised based on, the interior formulation. Traditionally, the domain is padded with zeros to prevent reflections in OWWE migration. However, this method only delays the reflections. Moreover, it increases

Manuscript received by the Editor December 8, 2004; revised manuscript received June 2, 2005; published online May 24, 2006.
[1]Atlantia Offshore Ltd., 1255 Enclave Parkway, Suite 600, Houston, Texas 77077. E-mail: hheidari@atlantia.com.
[2]North Carolina State University, Department of Civil Engineering, 208 Mann Hall, Stinson Drive, Raleigh, North Carolina 27695-7908. E-mail: mnguddat@eos.ncsu.edu.

computing costs because of the increased domain size. Therefore, accurate ABCs developed specifically for OWWEs are desirable for accurate one-way modeling and migration.

A relatively small number of ABCs have been developed for OWWEs, based on both material and differential equation-based approaches. Clayton and Engquist (1980) introduced three local ABCs of varying accuracy (15° and 45° wave equations), extended by Zhou and McMechan (2000) to 3D migration. These methods are limited in that their accuracy cannot be increased readily and they are not applicable to high-order OWWEs. In fact, Howell and Trefethen (1988) show that any boundary condition of the Clayton-Engquist type of order higher than one is ill posed for migration equations of an order higher than three. In addition to these local ABCs, there have been some developments related to nonlocal ABCs (e.g., Papadakis, 1994; Thomson and Mayfield, 1994; Levy, 1997; Yevick and Thomson, 1999; Brooke and Thomson, 2000). Similar to their counterparts for full wave equations, these methods tend to be very expensive because of their global nature. PML-based methods have also been developed for OWWEs but are limited to frequency-domain computations (Collino, 1997; Yevick and Thomson, 2000; Levy, 2001).

In this paper, we derive systematically a series of arbitrarily accurate local ABCs applicable to high-order OWWEs in the time-domain as well as in the frequency domain. We develop ABCs that can be used in conjunction with a variety of wide-angle wave equations, based on the ideas of arbitrarily wide-angle wave equations (AWWEs) (Guddati, 2006). A stable explicit finite-difference scheme is devised for the time-domain implementation of downward continuation as modified by these ABCs. The effectiveness of the proposed ABCs is illustrated using various modeling and migration problems. We also note that the frequency-domain versions of the proposed ABCs provide a more efficient alternative to PML-based techniques.

First, we define the framework of the OWWEs for which the ABCs are devised. We then outline the basic concepts of the proposed ABCs, precisely derive the ABCs for modeling and migration, and perform a theoretical accuracy analysis through reflection coefficients. In the subsequent section, we develop a stable explicit finite-difference scheme for the time-domain implementation of the ABCs. Finally, we illustrate the performance of the ABCs by applying them to wide-angle wave propagation and AWWE migration (Guddati and Heidari, 2005).

THEORY

We start from a general form of high-order, upward-propagating OWWEs:

$$\mathbf{C}_1\frac{\partial^2\mathbf{u}}{\partial z\partial t}+\mathbf{C}_2\frac{\partial^2\mathbf{u}}{\partial t^2}+\mathbf{C}_3\frac{\partial^2\mathbf{u}}{\partial x^2}=\mathbf{0}, \tag{1}$$

where $\mathbf{C}_{1,2,3}$ are coefficient matrices, t is time, and

$$\mathbf{u}=\left[u\ u^1\ \cdots\ u^{n-1}\right]^T. \tag{2}$$

Here, u is the field variable, u^1 to u^{n-1} are the auxiliary variables, and T denotes transpose. Equation 1 is defined over $\{-\infty<x<\infty\}\times\{0<z<\infty\}\times\{0<t<\infty\}$. Examples of OWWEs that fit into equation 1 are (a) the 15° wave equation, which is obtained by setting $n=1$, $\mathbf{C}_1=1$, $\mathbf{C}_2=-1/c$, and $\mathbf{C}_3=c/2$; (b) the high-order paraxial (one-way) wave equation, introduced by Bamberger et al. (1988); and (c) the AWWE, developed by Guddati (2006). The AWWE formulation follows the form of equation 1, with the coefficient matrices presented in Appendix A. The high-order paraxial wave equation of Bamberger et al. (1988), on the other hand, is originally presented in a different form; but as shown in Appendix B, it can be modified to fit into equation 1.

For the solution of equation 1 to be computationally feasible, the domain is truncated in the x-direction to a finite domain, $0<x<x_{\max}$, referred to as the interior. The rest of the domain is called the exterior, which consists of two half-spaces, $x\le 0$ and $x\ge x_{\max}$. Once truncated, appropriate boundary conditions must be used at the truncation boundaries, namely, at $x=0$ (left boundary) and $x=x_{\max}$ (right boundary). For the solution in the truncated domain to be accurate, these boundary conditions must absorb any incident energy and prevent spurious reflections; hence, they are labeled ABC. Our goal is to derive a highly accurate version of these ABCs for high-order OWWEs, as defined in equation 1.

Formulation of the proposed ABC

Ideally, an ABC should exactly represent the effect of the half-space it is replacing. In the context of acoustic media, the ABC can be viewed as the representation of half-space impedance. The effective approximation of half-space impedance, explored in the derivation of AWWEs by Guddati, (2006), involves efficient finite-element discretization of the half-space. We closely follow these ideas in developing our proposed ABCs. The steps involved in this procedure are summarized below and are elaborated upon later in this section.

First, the half-space (exterior) is discretized using an infinite number of finite elements; this introduces error in the impedance. It turns out that this impedance error can be completely eliminated if the midpoint integration is utilized for the numerical integration of finite-element matrices [see Guddati (2006) for the proof]. Midpoint integration, explained in Appendix C (see equation C-7), ensures that the discretized half-space is equivalent to the original one, which enables the use of arbitrary lengths for the elements without concern over the accuracy of the discretization. Since an infinite number of elements cannot be used for computation, the discretized half-space is truncated, thus limiting the number of finite elements, and the Dirichlet boundary condition is applied on the truncation boundary. Owing to the midpoint integration, no reflections appear from any of the nodes between the boundary point and the truncation point. However, the truncation point itself generates reflections, introducing errors in the impedance. The error attributable to the reflections can be reduced significantly if the element lengths are chosen as complex or imaginary numbers. Guddati (2006) shows that, with such a choice, the half-space becomes the perfect propagator and thus a perfect absorber for wave modes with wavenumbers $k=2i/L_q$, where L_q is the length of the qth elements in the half-space. In addition to being a perfect absorber for these specific wave modes, the half-space (exterior) becomes an effective absorber for other waves as well. Summarizing, the exterior (half-space) is efficiently discretized using a limited number of finite elements, with the key being the use of midpoint integration along with imaginary element lengths.

The interior, in contrast to the exterior, is typically discretized using the finite-difference method. However, finite-difference discretization is equivalent to finite-element discretization if nodal-

point integration is used (see equations 14 and 15). Thus, since both the interior and the exterior fit into the framework of finite elements, we may now start with the finite-element discretization of equation 1 over the entire domain in the x-direction, i.e., $-\infty < x < \infty$. Since the discretization at this stage is only in the x-direction, it is more convenient to work with the Fourier-transformed version of equation 1:

$$(\omega k_z \mathbf{C}_1 - \omega^2 \mathbf{C}_2)\hat{\mathbf{u}} + \mathbf{C}_3 \frac{\partial^2 \hat{\mathbf{u}}}{\partial x^2} = \mathbf{0}, \tag{3}$$

where $\hat{\mathbf{u}} = \hat{\mathbf{u}}(\omega, k_z, x)$ is the Fourier transform of $\mathbf{u}$, ω is the wave frequency, and k_z is the vertical wavenumber (that is, the wavenumber along the preferred direction). Note that the sign convention for the Fourier transform is chosen such that the following dualities apply: $\partial/\partial t \leftrightarrow -i\omega$ and $\partial/\partial z \leftrightarrow ik_z$. The first step of the finite-element discretization is to obtain the variational form of equation 3 by multiplying the equation by an arbitrary function (the virtual field variable $\boldsymbol{\delta\hat{u}}$) and integrating the resulting expression over the entire domain, i.e., $-\infty < x < +\infty$. This results in

$$\int_{-\infty}^{+\infty} \boldsymbol{\delta\hat{\mathbf{u}}}^T \left[(\omega k_z \mathbf{C}_1 - \omega^2 \mathbf{C}_2)\hat{\mathbf{u}} + \mathbf{C}_3 \frac{\partial^2 \hat{\mathbf{u}}}{\partial x^2} \right] dx = 0 \quad \text{for all } \boldsymbol{\delta\hat{\mathbf{u}}}. \tag{4}$$

Performing integration by parts on the second term of equation 4 results in

$$\int_{-\infty}^{+\infty} \left[\boldsymbol{\delta\hat{\mathbf{u}}}^T (\omega k_z \mathbf{C}_1 - \omega^2 \mathbf{C}_2)\hat{\mathbf{u}} - \frac{\partial \boldsymbol{\delta\hat{\mathbf{u}}}^T}{\partial x} \mathbf{C}_3 \frac{\partial \hat{\mathbf{u}}}{\partial x} \right] dx = 0. \tag{5}$$

The domain is now discretized into an infinite number of finite elements, with the qth element defined as $[x_q, x_{q+1}]$. We number the elements such that $-\infty < q < 0$ corresponds to elements in the left half-space, $0 \le q < N_x$ corresponds to the interior elements, and $N_x \le q < +\infty$ corresponds to the elements in the right half-space. The integral in equation 5 can be divided into integrals over each of the finite elements as

$$\sum_{q=-\infty}^{q=+\infty} \left\{ \int_{x_q}^{x_{q+1}} \left[\boldsymbol{\delta\hat{\mathbf{u}}}^T (\omega k_z \mathbf{C}_1 - \omega^2 \mathbf{C}_2)\hat{\mathbf{u}} - \frac{\partial \boldsymbol{\delta\hat{\mathbf{u}}}^T}{\partial x} \mathbf{C}_3 \frac{\partial \hat{\mathbf{u}}}{\partial x} \right] dx \right\} = 0. \tag{6}$$

Following the Bubnov-Galerkin approach (see, e.g., Becker et al., 1981), the field variable and the virtual field variable are approximated in each element as

$$\hat{\mathbf{u}}(x) \approx \mathbf{N}(x) \begin{bmatrix} \hat{\mathbf{u}}_q \\ \hat{\mathbf{u}}_{q+1} \end{bmatrix}_{2n\times 1} \quad \text{and}$$

$$\boldsymbol{\delta\hat{\mathbf{u}}}(x) \approx \mathbf{N}(x) \begin{bmatrix} \boldsymbol{\delta\hat{\mathbf{u}}}_q \\ \boldsymbol{\delta\hat{\mathbf{u}}}_{q+1} \end{bmatrix}_{2n\times 1}, \tag{7}$$

where $\mathbf{N}(x)$ is the interpolation (shape) function, defined as

$$\mathbf{N}_q(x) = \left[\left(\frac{x_{q+1} - x}{L_q} \right) \mathbf{I} \left(\frac{x - x_q}{L_q} \right) \mathbf{I} \right]_{n\times 2n}. \tag{8}$$

Here, $\mathbf{I}$ is the identity matrix of size $n \times n$, and $L_q = x_{q+1} - x_q$ is the length of the qth element. Substituting equation 7 into equation 6 results in the discrete variational form

$$\sum_{q=-\infty}^{q=+\infty} \boldsymbol{\delta\hat{\mathbf{U}}}_q \hat{\mathbf{S}}_q \hat{\mathbf{U}}_q = 0, \tag{9}$$

where $\hat{\mathbf{U}}_q$ and $\boldsymbol{\delta\hat{\mathbf{U}}}_q$ are vectors of nodal values defined as

$$\hat{\mathbf{U}}_q = \begin{bmatrix} \hat{\mathbf{u}}_q \\ \hat{\mathbf{u}}_{q+1} \end{bmatrix}_{2n\times 1} \quad \text{and} \quad \boldsymbol{\delta\hat{\mathbf{U}}}_q = \begin{bmatrix} \boldsymbol{\delta\hat{\mathbf{u}}}_q \\ \boldsymbol{\delta\hat{\mathbf{u}}}_{q+1} \end{bmatrix}_{2n\times 1}. \tag{10}$$

The term $\hat{\mathbf{S}}_q \left(\equiv \begin{bmatrix} \hat{\mathbf{S}}_q^{11} & \hat{\mathbf{S}}_q^{12} \\ \hat{\mathbf{S}}_q^{21} & \hat{\mathbf{S}}_q^{22} \end{bmatrix} \right)$ is the stiffness of the qth element and is defined as

$$\hat{\mathbf{S}}_q = \left(\int_{x_q}^{x_{q+1}} \mathbf{N}_q^T (\omega k_z \mathbf{C}_1 - \omega^2 \mathbf{C}_2) \mathbf{N}_q dx \right) - \left(\int_{x_q}^{x_{q+1}} \frac{\partial \mathbf{N}_q}{\partial x}^T \mathbf{C}_3 \frac{\partial \mathbf{N}_q}{\partial x} dx \right). \tag{11}$$

We now continue with equation 9, which can be rearranged and written as

$$\begin{Bmatrix} \vdots \\ \boldsymbol{\delta\hat{\mathbf{u}}}_{q-1} \\ \boldsymbol{\delta\hat{\mathbf{u}}}_q \\ \boldsymbol{\delta\hat{\mathbf{u}}}_{q+1} \\ \vdots \end{Bmatrix} \begin{bmatrix} \ddots & \ddots & 0 & 0 & 0 \\ \ddots & \hat{\mathbf{S}}_{q-2}^{22} + \hat{\mathbf{S}}_{q-1}^{11} & \hat{\mathbf{S}}_{q-1}^{12} & 0 & 0 \\ 0 & \hat{\mathbf{S}}_{q-1}^{21} & \hat{\mathbf{S}}_{q-1}^{22} + \hat{\mathbf{S}}_q^{11} & \hat{\mathbf{S}}_q^{12} & 0 \\ 0 & 0 & \hat{\mathbf{S}}_q^{21} & \hat{\mathbf{S}}_q^{22} + \hat{\mathbf{S}}_{q+1}^{11} & \ddots \\ 0 & 0 & 0 & \ddots & \ddots \end{bmatrix} \times \begin{Bmatrix} \vdots \\ \hat{\mathbf{u}}_{q-1} \\ \hat{\mathbf{u}}_q \\ \hat{\mathbf{u}}_{q+1} \\ \vdots \end{Bmatrix} = \mathbf{0}. \tag{12}$$

Since equation 12 should hold true for any virtual field variable vector, it is equivalent to the linear system of equations given by

$$\begin{bmatrix} \ddots & \ddots & 0 & 0 & 0 \\ \ddots & \hat{\mathbf{S}}^{22}_{q-2} + \hat{\mathbf{S}}^{11}_{q-1} & \hat{\mathbf{S}}^{12}_{q-1} & 0 & 0 \\ 0 & \hat{\mathbf{S}}^{21}_{q-1} & \hat{\mathbf{S}}^{22}_{q-1} + \hat{\mathbf{S}}^{11}_{q} & \hat{\mathbf{S}}^{12}_{q} & 0 \\ 0 & 0 & \hat{\mathbf{S}}^{21}_{q} & \hat{\mathbf{S}}^{22}_{q} + \hat{\mathbf{S}}^{11}_{q+1} & \ddots \\ 0 & 0 & 0 & \ddots & \ddots \end{bmatrix} \begin{Bmatrix} \vdots \\ \hat{\mathbf{u}}_{q-1} \\ \hat{\mathbf{u}}_{q} \\ \hat{\mathbf{u}}_{q+1} \\ \vdots \end{Bmatrix} = \mathbf{0}. \tag{13}$$

Before moving on to the derivation of the boundary condition, note that the finite-element discretization of the interior is equivalent to the finite-difference discretization that is commonplace in the geophysics community. As mentioned before, the stiffness matrix for the interior elements is evaluated using nodal-point integration, resulting in

$$\hat{\mathbf{S}}_q = \frac{\Delta x}{2}(\omega k_z \mathbf{C}_1 - \omega^2 \mathbf{C}_2) * \begin{bmatrix} +1 & 0 \\ 0 & +1 \end{bmatrix} - \frac{1}{\Delta x}\mathbf{C}_3 * \begin{bmatrix} +1 & -1 \\ -1 & +1 \end{bmatrix}, \quad 0 \le q < N_x, \tag{14}$$

where Δx is the grid length in the x-direction. Note that nodal-point integration is necessary to obtain an uncoupled system of equations that enables explicit computation. See Appendix C for the details of derivation and the definition of the $*$ operator.

Examining the qth equation in the system of equations 13, we have

$$\hat{\mathbf{S}}^{21}_{q-1}\hat{\mathbf{u}}_{q-1} + (\hat{\mathbf{S}}^{22}_{q-1} + \hat{\mathbf{S}}^{11}_{q})\hat{\mathbf{u}}_q + \hat{\mathbf{S}}^{12}_{q}\hat{\mathbf{u}}_{q+1} = 0. \tag{15}$$

Substituting equation 14 into equation 15 leads to

$$(\omega k_z \mathbf{C}_1 - \omega^2 \mathbf{C}_2)\hat{\mathbf{u}}_q + \mathbf{C}_3 \frac{\hat{\mathbf{u}}_{q-1} - 2\hat{\mathbf{u}}_q + \hat{\mathbf{u}}_{q+1}}{\Delta x^2} = 0, \tag{16}$$

which is the central difference approximation of equation 3.

We now develop the ABCs for the left boundary. (Note that the right boundary can be derived in a similar way.) To write the boundary condition at the left, the equation corresponding to the points $x_{-\infty}$ to x_0 is written as

$$\begin{bmatrix} \ddots & \ddots & 0 & 0 \\ \ddots & \hat{\mathbf{S}}^{22}_{-3} + \hat{\mathbf{S}}^{11}_{-2} & \hat{\mathbf{S}}^{12}_{-2} & 0 \\ 0 & \hat{\mathbf{S}}^{21}_{-2} & \hat{\mathbf{S}}^{22}_{-2} + \hat{\mathbf{S}}^{11}_{-1} & \hat{\mathbf{S}}^{12}_{-1} \\ 0 & 0 & \hat{\mathbf{S}}^{21}_{-1} & \hat{\mathbf{S}}^{22}_{-1} + \hat{\mathbf{S}}^{11}_{0} \end{bmatrix} \begin{Bmatrix} \vdots \\ \hat{\mathbf{u}}_{-2} \\ \hat{\mathbf{u}}_{-1} \\ \hat{\mathbf{u}}_{0} \end{Bmatrix} = \begin{Bmatrix} \vdots \\ \mathbf{0} \\ \mathbf{0} \\ -\hat{\mathbf{S}}^{12}_{0}\hat{\mathbf{u}}_1 \end{Bmatrix}. \tag{17}$$

In equation 17, the right-hand side contains the contribution from the interior ($-\hat{\mathbf{S}}^{12}_0\hat{\mathbf{u}}_i$). As mentioned earlier in this section, in contrast to the interior, the midpoint integration is used to calculate the stiffness matrix for the exterior elements (see Appendix C for details), resulting in

$$\hat{\mathbf{S}}_q = \frac{L^e_q}{4}(\omega k_z \mathbf{C}_1 - \omega^2 \mathbf{C}_2) * \begin{bmatrix} +1 & +1 \\ +1 & +1 \end{bmatrix} - \frac{1}{L^e_q}\mathbf{C}_3 * \begin{bmatrix} +1 & -1 \\ -1 & +1 \end{bmatrix}, \quad q < 0 \text{ or } q \ge N_x, \tag{18}$$

where L^e_q is the length of each exterior element.

At this stage, equations 17 and 18 constitute the exact boundary condition, as the discretization error is eliminated using midpoint integration. However, in practice, one cannot solve equation 17 because it contains an infinite number of unknowns. Hence, the number of elements in the exterior is limited to m, with the Dirichlet boundary condition applied at the leftmost point, x_{-m}, i.e., $\hat{\mathbf{u}}_{-m} = \mathbf{0}$. Equation 17 then transforms into

$$\begin{bmatrix} \hat{\mathbf{S}}^{22}_{-m} + \hat{\mathbf{S}}^{11}_{-(m-1)} & \hat{\mathbf{S}}^{12}_{-(m-1)} & & \\ \hat{\mathbf{S}}^{21}_{-(m-1)} & \hat{\mathbf{S}}^{22}_{-(m-1)} + \hat{\mathbf{S}}^{11}_{-(m-2)} & \ddots & \\ & \ddots & \ddots & \hat{\mathbf{S}}^{12}_{-1} \\ & & \hat{\mathbf{S}}^{21}_{-1} & \hat{\mathbf{S}}^{22}_{-1} + \hat{\mathbf{S}}^{11}_{0} \end{bmatrix} \times \begin{Bmatrix} \hat{\mathbf{u}}_{-(m-1)} \\ \hat{\mathbf{u}}_{-(m-2)} \\ \vdots \\ \hat{\mathbf{u}}_{0} \end{Bmatrix} = \begin{Bmatrix} \mathbf{0} \\ \mathbf{0} \\ \vdots \\ -\hat{\mathbf{S}}^{12}_{0}\hat{\mathbf{u}}_1 \end{Bmatrix}. \tag{19}$$

The Dirichlet boundary condition at the truncation point results in reflections. As discussed earlier, this reflection can be reduced by using imaginary element lengths. By using an imaginary element length of $L_q = 2i/k^x_q$ (Guddati, 2006), the qth element becomes a perfect absorber for wavefields with the horizontal wavenumber k^x_q. However, since our goal is time-domain analysis, it is more convenient to deal with phase velocities than wavenumbers as the parameters of the ABC. Hence, we use the relationship between the wavenumber and the horizontal phase velocity, i.e., $k^x_q = \omega/c^x_q$, to obtain

$$L_q = \frac{2ic^x_q}{\omega}. \tag{20}$$

Substituting equation 20 into equation 18 results in the stiffness matrix of the absorbing elements:

$$\hat{\mathbf{S}}_q = \frac{ic^x_q}{2\omega}(\omega k_z \mathbf{C}_1 - \omega^2 \mathbf{C}_2) * \begin{bmatrix} +1 & +1 \\ +1 & +1 \end{bmatrix} - \frac{\omega}{2ic^x_q}\mathbf{C}_3 * \begin{bmatrix} +1 & -1 \\ -1 & +1 \end{bmatrix}, \quad q < 0 \text{ or } q \ge N_x. \tag{21}$$

Substituting equations 14 and 21 into equation 19 results in the final form of the absorbing boundary condition:

$$[(ik_z\mathbf{C}_1 - i\omega\mathbf{C}_2) * \boldsymbol{\Omega}_2 + i\omega\mathbf{C}_3 * \boldsymbol{\Omega}_1]\hat{\mathbf{U}} + \Delta x[(\omega k_z\mathbf{C}_1 - \omega^2\mathbf{C}_2) * \boldsymbol{\Omega}_3]\hat{\mathbf{U}} - \frac{2}{\Delta x}[\mathbf{C}_3 * \boldsymbol{\Omega}_3](\hat{\mathbf{U}} - \hat{\mathbf{U}}') = 0, \tag{22}$$

where

$$\boldsymbol{\Omega}_1 = \begin{bmatrix} \frac{1}{c^x_m} + \frac{1}{c^x_{m-1}} & \frac{-1}{c^x_{m-1}} & & & & \\ \frac{-1}{c^x_{m-1}} & \frac{1}{c^x_{m-1}} + \frac{1}{c^x_{m-2}} & \frac{-1}{c^x_{m-2}} & & & \\ & \frac{-1}{c^x_{m-2}} & \ddots & \ddots & & \\ & & \ddots & \frac{1}{c^x_2} + \frac{1}{c^x_1} & \frac{-1}{c^x_1} & \\ & & & \frac{-1}{c^x_1} & \frac{1}{c^x_1} & \end{bmatrix}_{m\times m}, \tag{23}$$

$$\boldsymbol{\Omega}_2 = \begin{bmatrix} c^x_m + c^x_{m-1} & c^x_{m-1} & & & & \\ c^x_{m-1} & c^x_{m-1} + c^x_{m-2} & c^x_{m-2} & & & \\ & c^x_{m-2} & \ddots & \ddots & & \\ & & \ddots & c^x_2 + c^x_1 & c^x_1 & \\ & & & c^x_1 & c^x_1 & \end{bmatrix}_{m\times m}, \tag{24}$$

$$\boldsymbol{\Omega}_3 = \begin{bmatrix} 0 & \cdots & & 0 \\ \vdots & \ddots & & \vdots \\ & & 0 & 0 \\ 0 & \cdots & 0 & 1 \end{bmatrix}, \tag{25}$$

$$\hat{\mathbf{U}} = \begin{Bmatrix} \hat{\mathbf{u}}_{-m} \\ \hat{\mathbf{u}}_{-m+1} \\ \vdots \\ \hat{\mathbf{u}}_0 \end{Bmatrix}, \quad \text{and } \hat{\mathbf{U}}' = \begin{Bmatrix} \mathbf{0} \\ \mathbf{0} \\ \vdots \\ \hat{\mathbf{u}}_1 \end{Bmatrix}. \tag{26}$$

Note that in equations 23 and 24 the phase velocity parameters are indexed with positive numbers for simplicity. Transforming equation 22 back into the time domain yields

$$(\mathbf{C}_1 * \boldsymbol{\Omega}_2)\frac{\partial\mathbf{U}}{\partial z} + (\mathbf{C}_2 * \boldsymbol{\Omega}_2 - \mathbf{C}_3 * \boldsymbol{\Omega}_1)\frac{\partial\mathbf{U}}{\partial t} + \Delta x(\mathbf{C}_1 * \boldsymbol{\Omega}_3)\frac{\partial^2\mathbf{U}}{\partial z\partial t} + \Delta x(\mathbf{C}_2 * \boldsymbol{\Omega}_3)\frac{\partial^2\mathbf{U}}{\partial t^2} - \frac{2}{\Delta x}(\mathbf{C}_3 * \boldsymbol{\Omega}_3)(\mathbf{U} - \mathbf{U}') = 0. \tag{27}$$

Equation 27 is the equation for an m-layer ABC with a parameter set of $(c^x_1, c^x_2, \ldots, c^x_m)$. This equation is readily extendible to straight boundaries in 3D domains by applying the above concepts to the coordinate perpendicular to the boundary. The terms related to the horizontal coordinate along the boundary are treated similarly to the interior. On the other hand, the treatment of the corners, where the ABC should absorb in both horizontal directions, needs careful attention and is beyond the scope of this paper. The ideas related to corner ABCs for full wave equations (Guddati and Lim, 2006) could be utilized for this purpose.

Extension to the migration problem

In the derivation of equation 27, we assume that the governing equation 3 is solved in positive time, i.e., as a forward problem. However, for the migration problem, the governing equation is the adjoint and is solved in reverse time. Therefore, for the boundary condition to have the same absorbing effect as in the forward problem, the wave frequency ω in equation 20 should be replaced by $-\omega$, which is equivalent to negating L^e_q. Consequently, based on equation 18, the contribution from the absorbing elements, i.e., the first two terms of equation 27, will change sign. Thus, equation 27 can be written in a more general form that will hold true for both forward and reverse (migration) problems:

$$\zeta\left[(\mathbf{C}_1 * \boldsymbol{\Omega}_2)\frac{\partial\mathbf{U}}{\partial z} + (\mathbf{C}_2 * \boldsymbol{\Omega}_2 - \mathbf{C}_3 * \boldsymbol{\Omega}_1)\frac{\partial\mathbf{U}}{\partial t}\right] + \Delta x(\mathbf{C}_1 * \boldsymbol{\Omega}_3)\frac{\partial^2\mathbf{U}}{\partial z\partial t} + \Delta x(\mathbf{C}_2 * \boldsymbol{\Omega}_3)\frac{\partial^2\mathbf{U}}{\partial t^2} - \frac{2}{\Delta x}(\mathbf{C}_3 * \boldsymbol{\Omega}_3)(\mathbf{U} - \mathbf{U}') = 0, \tag{28}$$

where

$$\zeta = \begin{cases} +1, & \text{forward problem} \\ -1, & \text{inverse problem (migration).} \end{cases} \tag{29}$$

Accuracy of a high-order ABC

The accuracy of an ABC is measured in terms of reflection coefficients. The reflection coefficient R of an ABC is defined as the ratio of the amplitude of the reflected wave to that of the original wave impinging on the boundary. Given an incident monochromatic wavefield u_{inc} moving toward the left boundary,

$$u_{\text{inc}} = e^{ik_z z - i\omega t}e^{-ik_x x}, \tag{30}$$

the total wavefield after reflecting from the boundary can be written as

$$u = e^{ik_z z - i\omega t}\left(e^{-ik_x x} + \mathrm{Re}^{ik_x x}\right). \tag{31}$$

The boundary condition for the governing equation 1 on the left ($x = 0$) can be written formally as

$$\left.\frac{\partial u}{\partial x}\right|_{x=0} + \left.\mathcal{B}u\right|_{x=0} = 0, \tag{32}$$

where $\mathcal{B}$ denotes a differential (or algebraic, if in the Fourier domain) operator. Substituting the total wavefield from equation 31 into equation 32 and rearranging yields

$$R = \frac{ik_x - \mathcal{B}}{ik_x + \mathcal{B}}. \tag{33}$$

At this point, the estimation of the reflection coefficient for the proposed ABC is reduced to finding the operator $\mathcal{B}$. The high-order OWWE (equation 1) approaches the exact OWWE as the number of auxiliary variables increases. Hence, to study the behavior of the reflection coefficient, it is appropriate to have the interior governed by the exact OWWE. Such an equation can be constructed from equation 3 by setting $\mathbf{C}_3 = 1$ and $(\omega k_z \mathbf{C}_1 - \omega^2 \mathbf{C}_2) = k_x^2$. Substituting these values into the general expression for the ABC in equation 22, we have

$$\left[\frac{ik_x^2}{\omega}\boldsymbol{\Omega}_2 + i\omega\boldsymbol{\Omega}_1\right]\hat{\mathbf{U}} + \Delta x[k_x^2\boldsymbol{\Omega}_3]\hat{\mathbf{U}} - \frac{2}{\Delta x}\boldsymbol{\Omega}_3(\hat{\mathbf{U}} - \hat{\mathbf{U}}') = 0. \tag{34}$$

Assuming that the discretization of the interior is very fine, we take the limit of equation 34 as $\Delta x \to 0$. Noting that $((\hat{\mathbf{U}}' - \hat{\mathbf{U}})/\Delta x) \to (\partial\hat{\mathbf{U}}/\partial x)$, equation 34 translates into

$$\boldsymbol{\Omega}_3\frac{\partial\hat{\mathbf{U}}}{\partial x} = \frac{1}{2}\left[\frac{ik_x^2}{\omega}\boldsymbol{\Omega}_2 + i\omega\boldsymbol{\Omega}_1\right]\hat{\mathbf{U}}. \tag{35}$$

Recalling the forms of $\boldsymbol{\Omega}_1$ and $\boldsymbol{\Omega}_2$, it is apparent that the matrix on the right-hand side of equation 35 is tridiagonal. Also, noting the form of $\boldsymbol{\Omega}_3$ in equation 25, equation 35 can be written as

$$\begin{Bmatrix} 0 \\ 0 \\ \vdots \\ 0 \\ \dfrac{\partial u_0}{\partial x} \end{Bmatrix} = \begin{bmatrix} a_{m+1} + a_m & b_m & & & \\ b_m & a_m + a_{m-1} & b_{m-1} & & \\ & b_{m-1} & \ddots & \ddots & \\ & & \ddots & a_2 + a_1 & b_1 \\ & & & b_1 & a_1 \end{bmatrix} \times \begin{Bmatrix} u_{-m} \\ u_{-m+1} \\ \vdots \\ u_{-1} \\ u_0 \end{Bmatrix}, \tag{36}$$

where u_0 is the value of u at the boundary,

$$a_j = \frac{1}{2}\left[\frac{ik_x^2 c_j^x}{\omega} + \frac{i\omega}{c_j^x}\right], \tag{37}$$

and

$$b_j = \frac{1}{2}\left[\frac{ik_x^2 c_j^x}{\omega} - \frac{i\omega}{c_j^x}\right]. \tag{38}$$

From equation 36, we can immediately conclude that all absorbing nodes $(u_{-m}, u_{-m+1}, \ldots, u_{-1})$ can be eliminated to arrive at the following expression in terms of the boundary point:

$$\frac{\partial u_0}{\partial x} = \mathcal{B}_m u_0, \tag{39}$$

where $\mathcal{B}_m$ is a continued fraction expansion, defined by

$$\mathcal{B}_m = a_m - \frac{b_m^2}{a_m + \mathcal{B}_{m-1}}. \tag{40}$$

Now we can return to equation 33 and write

$$R_m = \frac{ik_x + \mathcal{B}_m}{ik_x - \mathcal{B}_m}. \tag{41}$$

Substituting equation 40 into equation 41, noting that $a_m^2 - b_m^2 = -k_x^2$, results in the following recursive equation:

$$R_m = \left(\frac{a_m - ik_x}{a_m + ik_x}\right)\left(\frac{ik_x - \mathcal{B}_{m-1}}{ik_x + \mathcal{B}_{m-1}}\right) = \left(\frac{a_m - ik_x}{a_m + ik_x}\right)R_{m-1} \tag{42}$$

or

$$R_m = \prod_{j=1}^{m}\left(\frac{a_j - ik_x}{a_j + ik_x}\right). \tag{43}$$

Substituting the expression for a_j in equation 37 into equation 43 and rearranging will result in the final form of the reflection coefficient for the m-layer ABC:

$$R_m = \prod_{j=1}^{m}\left(\frac{c_j^x - c_x}{c_j^x + c_x}\right)^2. \tag{44}$$

We can obtain a more intuitive representation by noting that c_x can be written as $c/\sin\theta$, where θ is the angle of propagation with respect to the vertical axis (which is equal to 90° minus the angle of incidence on the lateral boundary) and c is the phase velocity. Similarly, we can write the phase velocity parameters as $c_j^x = c/\sin\theta_j$, where θ_j can be viewed as the parameters of the ABC. The reflection coefficient in equation 44 can then be rewritten as

$$R_m = \prod_{j=1}^{m}\left(\frac{\sin\theta_j - \sin\theta}{\sin\theta_j + \sin\theta}\right)^2. \tag{45}$$

Equation 45 can be used to intuitively design effective parameters of the proposed ABC. We can see from equation 45 that each θ_j indicates a particular value of θ for which the reflection coefficient becomes zero, i.e., the boundary condition becomes exact. Hence, the distribution of the reflection coefficient along the range $[0, 90°]$ can be adjusted by choosing the proper parameter set. This property is illustrated in Figure 1, where the reflection coefficient is shown for three different cases. By changing the parameter set in the second-order ABC from (90°, 90°) to (10°, 60°), the reflection coefficient becomes much smaller for lower incident angles. Note that 10° and 60° are not products of an optimization procedure but are chosen arbitrarily to scatter the zero points of the reflection coefficient along the $[0, 90°]$ range. By increasing the number of layers to three with reference angles $\theta_j = (5°, 20°, 60°)$, we achieved perfect absorption for propagation angles greater than 5°, clearly illustrating the flexibility and high accuracy of the proposed ABCs.

Remarks on frequency-domain implementation

The proposed ABCs can be readily extended to the frequency domain, which provides an efficient alternative to existing PML-based methods (see, e.g., Collino, 1997; Yevick and Thomson, 2000; Levy, 2001). The main difference between PML-based methods and the frequency-domain version of the proposed ABC is twofold: (1) We use purely imaginary lengths rather than the complex lengths used in the PML method, thus increasing the absorption of propagating waves (Asvadurov et al., 2003) and (2) in contrast to the approximate nature of PML discretization, we eliminate the discretization error through midpoint integration, thus enabling the use of arbitrarily large element lengths. Based on these desirable properties, we are able to achieve accurate absorption with just two additional gridpoints.

Remarks on evanescent modes

The proposed ABCs can be adjusted to absorb evanescent wave modes. Approximate OWWEs generate evanescent modes, which are not present in exact OWWEs (Bamberger et al., 1988). We can easily verify that for evanescent waves, $c_x < c$, which is equivalent to $\sin\theta > 1$ (complex θ_j). The proposed ABCs can be designed to absorb evanescent modes by choosing one or more of the phase velocity parameters to be less than c, i.e., by choosing one or more θ_j to be complex numbers.

Numerical implementation

We discretize the differential equation 28 in z and t in a manner consistent with the discretization performed for the AWWE in the interior (see Guddati and Heidari, 2005). Consider a grid in the z-t plane in which $z_j = j\Delta z$ and $t_k = k\Delta t$. The notation $\mathbf{U}_j^k$ denotes the value of the $\mathbf{U}$ vector at time t_k and depth z_j. We assume the surface to be located at $z = 0$, and z increases with depth, i.e., the z-axis points downward. We also assume that the disturbance is traveling toward the surface, i.e., upward. For the discretization in the z-direction, the Crank-Nicholson method is used. Hence, the equation is written for the midpoint of the layer, i.e., $z_{j+1/2} = (j + 1/2)\Delta z$, using the following approximations:

$$\mathbf{U}_{j+\frac{1}{2}} = \frac{1}{2}(\mathbf{U}_{j+1} + \mathbf{U}_j) \quad \text{and} \quad \left(\frac{\partial \mathbf{U}}{\partial z}\right)_{j+\frac{1}{2}} = \frac{\mathbf{U}_{j+1} - \mathbf{U}_j}{\Delta z}. \tag{46}$$

Such discretization of equation 28 results in

$$\zeta\left[\frac{1}{\Delta z}(\mathbf{C}_1 * \boldsymbol{\Omega}_2)(\mathbf{U}_{j+1} - \mathbf{U}_j) + (\mathbf{C}_2 * \boldsymbol{\Omega}_2 - \mathbf{C}_3 * \boldsymbol{\Omega}_1)\frac{\partial \mathbf{U}_{j+\frac{1}{2}}}{\partial t}\right] + \frac{\Delta x}{\Delta z}(\mathbf{C}_1 * \boldsymbol{\Omega}_3) \times \frac{\partial}{\partial t}(\mathbf{U}_{j+1} - \mathbf{U}_j) + \Delta x(\mathbf{C}_2 * \boldsymbol{\Omega}_3)\frac{\partial^2 \mathbf{U}_{j+\frac{1}{2}}}{\partial t^2} - \frac{2}{\Delta x}(\mathbf{C}_3 * \boldsymbol{\Omega}_3)(\mathbf{U}_{j+\frac{1}{2}} - \mathbf{U}'_{j+\frac{1}{2}}) = 0. \tag{47}$$

The next step is to discretize equation 47 in time. Again, to be consistent with the solution of the interior, the last three terms, i.e., the contributions of the interior, are discretized using the central-difference method. For the discretization in time, we propose a special averaging scheme that links the field variable in the exterior at any time instance to the average of the field variable in the interior for adjacent time steps, i.e.,

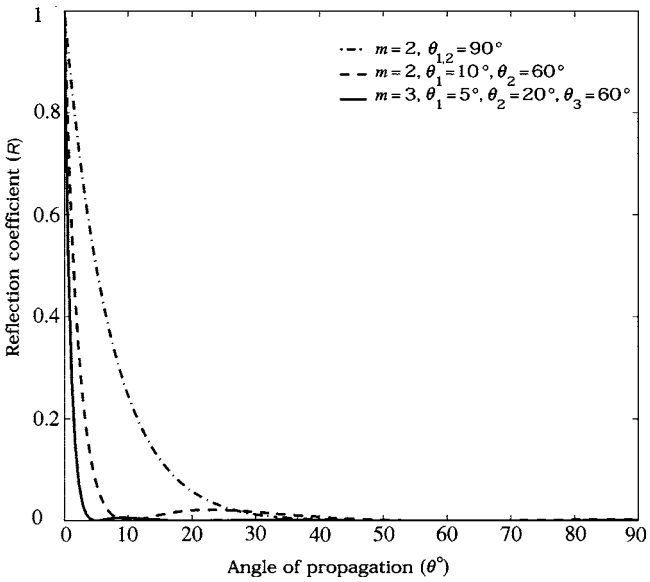

Figure 1. The reflection coefficient for the three different cases of the proposed ABC. The horizontal axis is the wave propagation angle, measured from the vertical axis i.e., waves traveling parallel to the boundary will have an angle of $\theta = 0°$. The dashed-dotted line represents the two-layer ABC with both phase velocity parameters set equal to the interior wave speed c (equivalent to $\theta_{1,2} = 90°$). By adjusting these two parameters to $\theta_1 = 10°$ and $\theta_2 = 60°$, the reflection coefficient becomes smaller for a wider range of incident angles (dashed line). The third-order ABC with a parameter set of $\theta_j = (5°, 20°, 60°)$, which corresponds to phase velocity parameters of $c_j^x = (11.5c, 2.92c, 1.15c)$, shows a nearly perfect reflection coefficient for any propagation angle greater than 5° (solid line).

$$\mathbf{U}^k = \tfrac{1}{2}(\mathbf{U}^{k+1} + \mathbf{U}^{k-1}) \tag{48}$$

is substituted in the first bracket of equation 47. This special finite-difference scheme is proposed to achieve stability in the numerical implementation of the ABC. The stability of the resulting scheme is verified through extensive computer-assisted stability analysis. The analytical proof of the stability is beyond the scope of this paper.

Substituting equation 48 into equation 47, along with temporal discretization, results in the following expression:

$$\begin{aligned}
&\zeta\Bigg[\frac{1}{2\Delta z}(\mathbf{C}_1 * \boldsymbol{\Omega}_2)(\mathbf{U}_{j+1}^{k+1} - \mathbf{U}_j^{k+1} + \mathbf{U}_{j+1}^{k-1} - \mathbf{U}_j^{k-1}) \\
&\quad + \frac{1}{2\Delta t}(\mathbf{C}_2 * \boldsymbol{\Omega}_2 - \mathbf{C}_3 * \boldsymbol{\Omega}_1)(\mathbf{U}_{j+\frac{1}{2}}^{k+1} - \mathbf{U}_{j+\frac{1}{2}}^{k-1})\Bigg] \\
&\quad + \frac{\Delta x}{2\Delta z \Delta t}(\mathbf{C}_1 * \boldsymbol{\Omega}_3)(\mathbf{U}_{j+1}^{k+1} - \mathbf{U}_j^{k+1} - \mathbf{U}_{j+1}^{k-1} + \mathbf{U}_j^{k-1}) \\
&\quad + \frac{\Delta x}{\Delta t^2}(\mathbf{C}_2 * \boldsymbol{\Omega}_3)(\mathbf{U}_{j+\frac{1}{2}}^{k+1} - 2\mathbf{U}_{j+\frac{1}{2}}^{k} + \mathbf{U}_{j+\frac{1}{2}}^{k-1}) \\
&\quad - \frac{2}{\Delta x}(\mathbf{C}_3 * \boldsymbol{\Omega}_3)(\mathbf{U}_{j+\frac{1}{2}}^{k} - \mathbf{U}_{j+\frac{1}{2}}^{\prime k}) = 0.
\end{aligned} \tag{49}$$

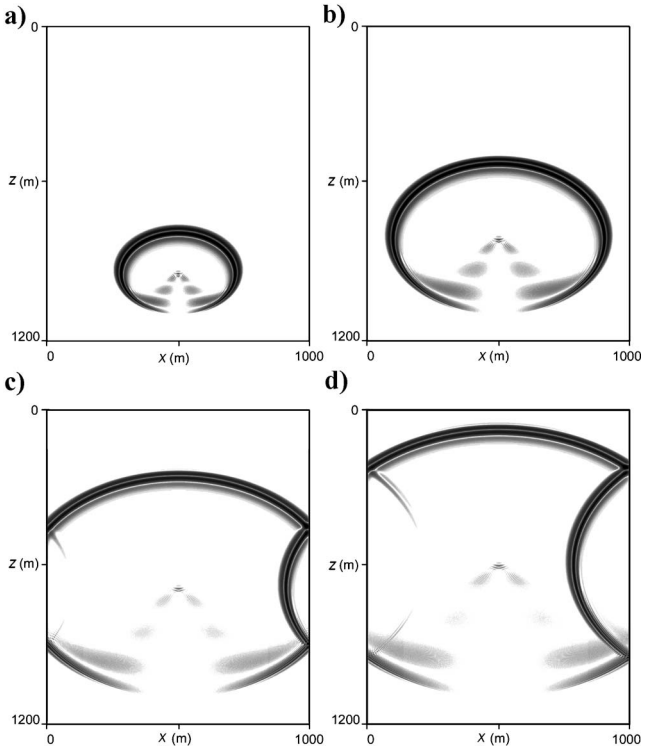

Figure 2. Four snapshots of a point source propagated by the 15° OWWE in a homogeneous domain (c = 4000 m/s): (a) 88 ms, (b) 154 ms, (c) 220 ms, and (d) 264 ms. The right edge of the domain is modeled as a rigid boundary. A single-layer ABC with c_x^1 = 2800 m/s is used on the left edge, which is expected to absorb waves traveling perpendicular to the boundary. Panels (c) and (d) clearly show that the absorption agrees with the theory.

For the forward problem, the solution procedure is to march upward in the z-direction to obtain $\mathbf{U}_j$ from $\mathbf{U}_{j+1}$ and forward in time (increasing k). This translates into obtaining $\mathbf{U}_{j+1/2}^{k+1}$ from equation 49 and eventually $\mathbf{U}_j^{k+1}$ from equation 46. For migration, on the other hand, this procedure is performed in reverse order on the same grid, i.e., we march downward in the z-direction (and obtain $\mathbf{U}_{j+1}$ from $\mathbf{U}_j$) and backward in time (decreasing k). Thus, the unknown variable in the migration problem is $\mathbf{U}_{j+1/2}^{k-1}$, which from equation 46 results in $\mathbf{U}_{j+1}^{k-1}$.

Based on the above procedures and following the details in Appendix D, the general discretized formula that holds true for both forward and migration problems can be expressed as

$$\begin{aligned}
\mathbf{U}_{j+\frac{1}{2}}^{k+\zeta} = \mathbf{B}_2(-\mathbf{U}_{j+\frac{1}{2}}^{k-\zeta} + \mathbf{U}_{j+\gamma}^{k+1} + \mathbf{U}_{j+\gamma}^{k-1}) + \mathbf{B}_3\mathbf{U}_{j+\frac{1}{2}}^{k-\zeta} + \mathbf{B}_4(\mathbf{U}_{j+\frac{1}{2}}^{k-\zeta} \\
+ \zeta\mathbf{U}_{j+\gamma}^{k+1} - \zeta\mathbf{U}_{j+\gamma}^{k-1}) + \mathbf{B}_5(-2\mathbf{U}_{j+\frac{1}{2}}^{k} + \mathbf{U}_{j+\frac{1}{2}}^{k-1}) \\
+ \mathbf{B}_6(\mathbf{U}_{j+\frac{1}{2}}^{k} - \mathbf{U}_{j+\frac{1}{2}}^{\prime k}),
\end{aligned} \tag{50}$$

where γ and ζ are problem-dependent flags ($\gamma = \zeta = 1$ for forward modeling; $\gamma = 0$ and $\zeta = -1$ for migration). The coefficient matrices $\mathbf{B}_1$ to $\mathbf{B}_6$ are defined in Appendix D. The difference equation 50 is written at the middle of the depth layers ($j + 1/2$) because the auxiliary variables are needed, calculated, and stored only at these locations. Such a strategy is critical to the efficiency of the time-domain implementation [see Guddati and Heidari (2005) for details].

NUMERICAL EXAMPLES

In this section, we investigate the performance of the proposed ABCs using numeric examples for both forward propagation and migration problems. To illustrate the accuracy properties derived earlier in the paper, we first use the proposed ABC in conjunction with the 15° equation (the lowest order AWWE). Figure 2 shows snapshots of a point source propagated using the 15° equation in a homogeneous medium (c = 4000 m/s). For the 15° equation, we see the phase velocity of horizontally propagating waves c_h is $c/\sqrt{2}$ or about 2800 m/s. The single-layer ABC is utilized on the left edge of the domain, while a Dirichlet boundary condition is used on the right edge. The phase velocity parameter of the ABC is set as $c_1^x = c_h$, which should result in perfect absorption of horizontally propagating waves. One can clearly see from Figures 2c and 2d that the wavefront impinging on the left boundary is absorbed better around the horizontally propagating region. A slight reflection can be seen on the bottom left and the top left of the front because the phase velocities of these regions differ considerably from c_h.

To investigate the effect of the reference phase velocity, the same problem (the 15° equation with the one-layer ABC) is analyzed with varying reference phase velocities. Figures 3a–3c show the snapshots at a particular instant (t = 264 ms) from these analyses. Figure 3a corresponds to c_1^x = 1000 m/s. Since the reference phase velocity is smaller than c_h, we expect the evanescent mode (the bottom wavefront) to be well absorbed, which is clearly seen in Figure 3a. Naturally, the rest of the wavefront results in some reflections. In Figure 3b, the snapshot for $c_1^x = c_h$ is repeated from Figure 2 for comparison. Figure 3c shows the case when c_1^x = 6000 m/s, which is larger than c_h. As expected, most of the top

left portion of the wavefront is absorbed. Finally, to illustrate the flexibility of the proposed ABC, a three-layer ABC with $c^x_{1,2,3}$ = (1000, 2800, 6000) m/s is utilized. The result is shown in Figure 3d, which effectively absorbs the entire wavefront.

Figure 4 illustrates the effectiveness of the proposed ABC for the AWWE equations. In this example, we consider a homogeneous domain with c = 2800 m/s along with a two-layer AWWE ($c_{1,2}$ = 4000, 8000 m/s) as the propagator. The forward propagation of a point source is shown in Figure 4 at four different time steps. Here, we utilize a three-layer ABC with $c^x_{1,2,3}$ = (1000, 2800, 6000) m/s on the left edge. With only three layers, practically all of the wavefront hitting the left edge is absorbed, including the evanescent modes.

To study the performance of the proposed ABC in migration, we (a) used a domain with a simple reflector, (b) generated the surface trace using the exploding reflector model (Loewenthal et al. 1976), (c) truncated the domain and, consequently, the surface trace, and (d) performed migration in the truncated domain with and without the absorbing boundary condition. We considered a homogeneous domain with a single dipping reflector (Figure 5) with a background velocity of c = 4000 m/s. After obtaining the surface trace using the exploding reflector model, we truncated the domain down to $x \in [600, 1600]$. The performance of the ABC can be assessed by imaging this model in the truncated domain. Since a portion of the truncated surface trace is associated with the portion of

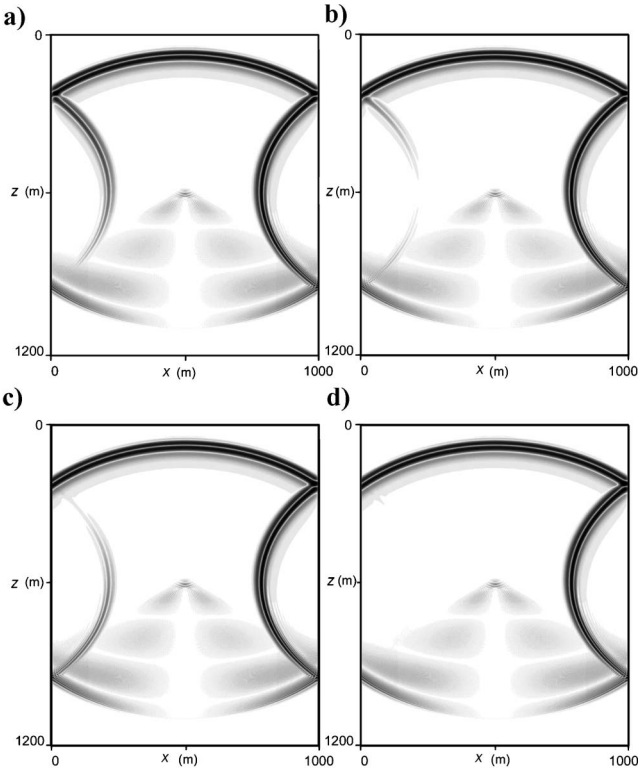

Figure 3. Snapshots of a point source propagated by the 15° OWWE in a homogeneous domain (c = 4000 m/s) at a particular time (t = 264 ms). The proposed ABC is implemented on the left edge with different orders and parameters in different panels. The right edge of the domain is modeled as a rigid boundary for all panels. (a) Single-layer ABC with c^1_x = 1000 m/s. With the phase velocity smaller than c^h, the absorption is good for the evanescent modes (the lower part of the propagation front). (b) Single-layer ABC with c^1_x = 2800 m/s (same as Figure 2; horizontally propagating waves are absorbed). (c) Single-layer ABC with c^1_x = 6000 m/s. The phase velocity is larger than that of horizontally propagating waves; hence, the top-left region of the wavefront is absorbed better. (d) Three-layer ABC with $c^x_{1,\,2,\,3}$ = 1000, 2800, 6000 m/s. By combining the effect of panels (a), (b), and (c), the boundary condition absorbs nearly all of the incident wavefront.

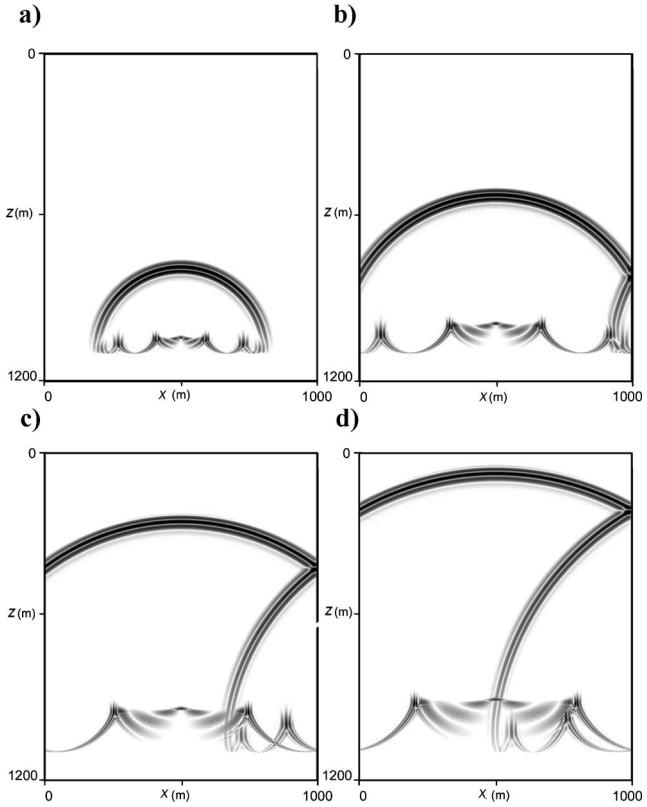

Figure 4. Four snapshots of a point-source disturbance propagating through a homogeneous domain (c = 4000 m/s) with the AWWE wide-angle wave equation: (a) 40 ms, (b) 154 ms, (c) 220 ms, and (d) 264 ms. The performance of the proposed ABC is illustrated for the AWWE propagator. A three-layer ABC with $c^x_{1,\,2,\,3}$ = 1000, 2800, 6000 m/s is used as the boundary condition for the left edge. The boundary condition absorbs all of the incident waves ranging from evanescent modes to the upper part of the wavefront.

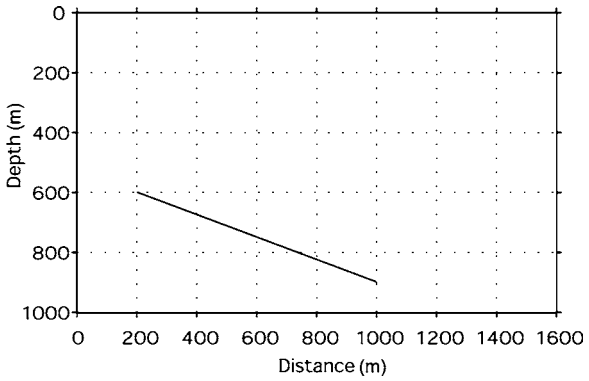

Figure 5. Synthetic model used for evaluating the proposed ABC in migration. The domain is assumed to be homogeneous with the background velocity of c = 4000 m/s.

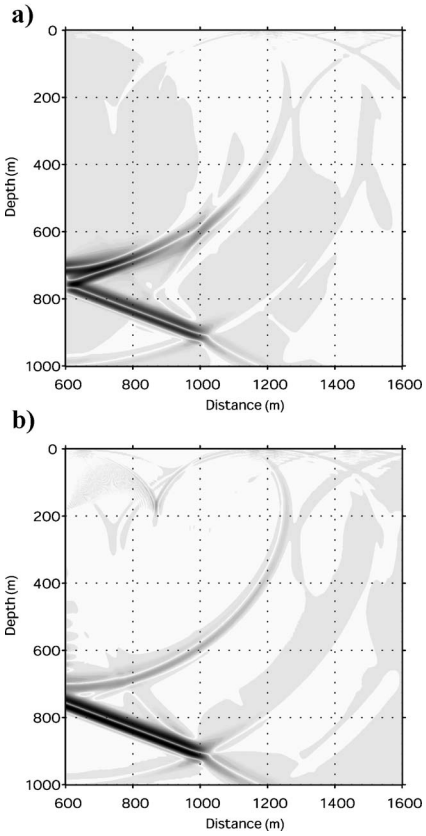

Figure 6. Migration in the truncated domain $x = [600, 1600]$ using (a) a rigid boundary on the left edge and (b) a three-layer ABC on the left edge. The rigid boundary results in artifacts, which are clearly eliminated when the three-layer ABC is used.

the reflector that is outside of the truncated domain, it should have some artifacts in the image if the left edge of the domain is modeled as a rigid boundary. Such artifacts come from the migration of the surface trace toward the outside of the truncated domain, which consequently hits the left boundary in the migration process and generates reflections that then appear as artifacts. Figure 6 shows the migration in the truncated domain. As expected, when no ABC is used on the left boundary, an artifact appears on the top of the image of the original reflector, as shown in Figure 6a. However, this artifact is completely eliminated in Figure 6b where a three-layer ABC is used with $c^x_{1,2,3} = 1000, 2800, 6000$ m/s, which shows the effectiveness of the proposed ABC in migration problems.

CONCLUSIONS

We have developed a highly accurate series of ABCs for modeling and migration with high-order OWWEs. These ABCs apply to any OWWE that fits into the framework of equation 1, such as the 15° wave equation, the high-order paraxial wave equation, or the scalar AWWE equations. The accuracy of the proposed boundary condition can be controlled by the number of absorbing elements and their phase velocity parameters. By distributing the parameters over the proper range of phase velocities, effective absorption of the entire wavefront can be achieved with very few layers. We have designed a special finite-difference scheme for time-domain explicit implementation of downward continuation with ABCs. Numerical examples clearly illustrate that reflection/artifact-free results can be obtained for both forward and migration problems with just three absorbing elements.

ACKNOWLEDGMENTS

This material is based upon work supported by the National Science Foundation under grant CMS-0100188. Any opinions, findings, and conclusions or recommendations expressed in this material are those of the authors and do not necessarily reflect the views of the National Science Foundation.

APPENDIX A

AWWE FORMULATION

The general framework of the AWWE equations is introduced in Guddati (2006), and the acoustic version is implemented in the context of migration in Guddati and Heidari (2005). The upward-propagating AWWE is formulated as the following system of equations:

$$\mathbf{d}\frac{\partial^2 \mathbf{u}}{\partial z \partial t} - \frac{1}{c}(\boldsymbol{\Lambda}_1 + \boldsymbol{\Lambda}_2)\frac{\partial^2 \mathbf{u}}{\partial t^2} + c\boldsymbol{\Lambda}_2\frac{\partial^2 \mathbf{u}}{\partial x^2} = \mathbf{0}, \quad \text{(A-1)}$$

where

$$\boldsymbol{\Lambda}_1 = \frac{c}{2}\begin{bmatrix} \frac{1}{c_1} & \frac{-1}{c_1} & & & & & \\ \frac{-1}{c_1} & \frac{1}{c_1}+\frac{1}{c_2} & \frac{-1}{c_2} & & & & \\ & \frac{-1}{c_2} & \ddots & \ddots & & & \\ & & \ddots & \frac{1}{c_{n-2}}+\frac{1}{c_{n-1}} & \frac{-1}{c_{n-1}} & & \\ & & & \frac{-1}{c_{n-1}} & \frac{1}{c_{n-1}}+\frac{1}{c_n} & \end{bmatrix}_{n\times n}, \quad \text{(A-2)}$$

$$\boldsymbol{\Lambda}_2 = \frac{1}{2c}\begin{bmatrix} c_1 & c_1 & & & & & \\ c_1 & c_1+c_2 & c_2 & & & & \\ & c_2 & \ddots & \ddots & & & \\ & & \ddots & c_{n-2}+c_{n-1} & c_{n-1} & & \\ & & & c_{n-1} & c_{n-1}+c_n & \end{bmatrix}_{n\times n}, \quad \text{(A-3)}$$

and

$$\mathbf{d} = \{1\ 0\ \cdots\ 0\}^T_{n\times 1}. \quad \text{(A-4)}$$

Where, n is the order of the AWWE and the parameters $c_{1,\ldots,n}$ are the phase velocities that can be used to control the accuracy of the AWWE. For details on the effects of n and c_i on AWWE accuracy, see Guddati and Heidari (2005).

APPENDIX B

COEFFICIENT MATRICES FOR BAMBERGER ET AL.'S HIGH-ORDER PARAXIAL EQUATION

The original form of the high-order, one-way (paraxial) wave equation, introduced by Bamberger et al. (1988), when modified for upward propagation is given by

$$\begin{cases} \dfrac{\partial^2 u}{\partial t \partial z} - \dfrac{1}{c}\dfrac{\partial^2 u}{\partial t^2} + \beta c \dfrac{\partial^2 u}{\partial x^2} + \dfrac{1}{c}\displaystyle\sum_{k=1}^{n-1} \beta_k \dfrac{\partial^2 \varphi_k}{\partial t^2} = 0, \\ -\dfrac{1}{c}\dfrac{\partial^2 \varphi_k}{\partial t^2} + c\gamma_k^2 \dfrac{\partial^2 \varphi_k}{\partial x^2} + c\dfrac{\partial^2 u}{\partial x^2} = 0 \end{cases} \tag{B-1}$$

for the $(n-1)^{\text{th}}$ order of approximation [see Bamberger et al. (1988) for the definition of parameters]. Defining $\mathbf{u}$ as

$$\mathbf{u} = [u \;\; \varphi_1 \;\; \varphi_2 \;\; \cdots \;\; \varphi_{n-1}]^T \tag{B-2}$$

and writing equation B-1 in the form of equation 1 yields the following coefficient matrices:

$$\mathbf{C}_1 = \begin{bmatrix} 1 & 0 & \cdots & 0 \\ 0 & 0 & & \vdots \\ \vdots & & \ddots & \\ 0 & \cdots & & 0 \end{bmatrix}, \tag{B-3}$$

$$\mathbf{C}_2 = -\frac{1}{c}\begin{bmatrix} 1 & -\beta_1 & -\beta_2 & \cdots & -\beta_{n-1} \\ & 1 & & & \\ & & 1 & & \\ & & & \ddots & \\ & & & & 1 \end{bmatrix}, \tag{B-4}$$

and

$$\mathbf{C}_3 = c\begin{bmatrix} \beta & & & & \\ 1 & \gamma_1^2 & & & \\ \vdots & & \gamma_2^2 & & \\ 1 & & & \ddots & \\ 1 & & & & \gamma_{n-1}^2 \end{bmatrix}. \tag{B-5}$$

APPENDIX C

CALCULATION OF THE STIFFNESS MATRICES FOR THE INTERIOR AND THE EXTERIOR

We start with equation 11

$$\hat{\mathbf{S}}_q = \left(\int_{x_q}^{x_{q+1}} \mathbf{N}_q^T (\omega k \mathbf{C}_1 - \omega^2 \mathbf{C}_2) \mathbf{N}_q dx \right) - \left(\int_{x_q}^{x_{q+1}} \frac{\partial \mathbf{N}_q^T}{\partial x} \mathbf{C}_3 \frac{\partial \mathbf{N}_q}{\partial x} dx \right). \tag{C-1}$$

Because the coefficient matrices $\mathbf{C}_{1,2,3}$ are independent of x, expression C-1 reduces to

$$\hat{\mathbf{S}}_q = (\omega k \mathbf{C}_1 - \omega^2 \mathbf{C}_2) * \left(\int_{x_q}^{x_{q+1}} \mathbf{N}_q^T \mathbf{N}_q dx \right) - \mathbf{C}_3 * \left(\int_{x_q}^{x_{q+1}} \frac{\partial \mathbf{N}_q^T}{\partial x} \frac{\partial \mathbf{N}_q}{\partial x} dx \right). \tag{C-2}$$

The $*$ operator is defined as follows: $\mathbf{A}_{n\times n} * \mathbf{B}_{m\times m}$ results in a matrix $\mathbf{C}_{mn\times mn}$ which is obtained by replacing each element of $\mathbf{B}$ by a submatrix $b_{ij}\mathbf{A}$. Assuming that $\mathbf{B}$ is a 2×2 matrix, we can write

$$\mathbf{A}_{n\times n} * \mathbf{B}_{2\times 2} = \begin{bmatrix} b_{11}\mathbf{A} & b_{12}\mathbf{A} \\ b_{21}\mathbf{A} & b_{22}\mathbf{A} \end{bmatrix}_{2n\times 2n}. \tag{C-3}$$

For the interior elements, the integrals in equation C-2 should be calculated using nodal-point integration (the trapezoidal rule), which results in

$$\int_{x_q}^{x_{q+1}} \mathbf{N}_q^T \mathbf{N}_q dx = \frac{L_q}{2}\left[\mathbf{N}_q^T \mathbf{N}_q|_{x_{q+1}} + \mathbf{N}_q^T \mathbf{N}_q|_{x_q} \right] = \frac{L_q}{2}\begin{bmatrix} +1 & 0 \\ 0 & +1 \end{bmatrix} \tag{C-4}$$

and, similarly,

$$\int_{x_q}^{x_{q+1}} \frac{\partial \mathbf{N}_q^T}{\partial x} \frac{\partial \mathbf{N}_q}{\partial x} dx = \frac{1}{L_q}\begin{bmatrix} +1 & -1 \\ -1 & +1 \end{bmatrix}. \tag{C-5}$$

For simplicity, assume a uniform grid in the x-direction for the interior, i.e., $L_q = \Delta x$. Hence, the stiffness for the interior elements becomes

$$\hat{\mathbf{S}}_q = \frac{\Delta x}{2}(\omega k \mathbf{C}_1 - \omega^2 \mathbf{C}_2) * \begin{bmatrix} +1 & 0 \\ 0 & +1 \end{bmatrix} - \frac{1}{\Delta x}\mathbf{C}_3 * \begin{bmatrix} +1 & -1 \\ -1 & +1 \end{bmatrix}, \quad 0 \le q < N_x. \tag{C-6}$$

On the other hand, for the exterior elements, we use midpoint integration, i.e.,

$$\int_a^b f(x)dx = (b-a) f\left(\frac{b+a}{2}\right), \tag{C-7}$$

which results in

$$\int_{x_q}^{x_{q+1}} \mathbf{N}_q^T \mathbf{N}_q dx = \frac{L_q^e}{4}\begin{bmatrix} +1 & +1 \\ +1 & +1 \end{bmatrix} \tag{C-8}$$

and

$$\int_{x_q}^{x_{q+1}} \frac{\partial \mathbf{N}_q^T}{\partial x}\frac{\partial \mathbf{N}_q}{\partial x} dx = \frac{1}{L_q^e}\begin{bmatrix} +1 & -1 \\ -1 & +1 \end{bmatrix}, \tag{C-9}$$

where L_q^e is the length of the exterior element q. Substituting equations C-8 and C-9 into equation C-2 results in the following stiffness matrix for the exterior elements:

$$\hat{\mathbf{S}}_q = \frac{L_q^e}{4}(\omega k \mathbf{C}_1 - \omega^2 \mathbf{C}_2) * \begin{bmatrix} +1 & +1 \\ +1 & +1 \end{bmatrix} - \frac{1}{L_q^e}\mathbf{C}_3 * \begin{bmatrix} +1 & -1 \\ -1 & +1 \end{bmatrix}, \quad q < 0 \text{ or } q \geq N_x. \tag{C-10}$$

APPENDIX D

THE FINITE-DIFFERENCE SCHEME

In the case of the forward problem, $\mathbf{U}_{j+1/2}^{k+1}$ should be obtained from the rest of the points in the stencil. Eliminating $\mathbf{U}_j$ in equation 49, based on equation 46, and rearranging for $\mathbf{U}_{j+1/2}^{k+1}$ results in

$$\mathbf{U}_{j+\frac{1}{2}}^{k+1} = \mathbf{B}_2(\mathbf{U}_{j+1}^{k+1} + \mathbf{U}_{j+1}^{k-1} - \mathbf{U}_{j+\frac{1}{2}}^{k-1}) + \mathbf{B}_3\mathbf{U}_{j+\frac{1}{2}}^{k-1} + \mathbf{B}_4(\mathbf{U}_{j+1}^{k+1} - \mathbf{U}_{j+1}^{k-1} + \mathbf{U}_{j+\frac{1}{2}}^{k-1}) + \mathbf{B}_5(-2\mathbf{U}_{j+\frac{1}{2}}^{k} + \mathbf{U}_{j+\frac{1}{2}}^{k-1}) + \mathbf{B}_6(\mathbf{U}_{j+\frac{1}{2}}^{k} - \mathbf{U}_{j+\frac{1}{2}}^{\prime k}), \tag{D-1}$$

where

$$\mathbf{B}_1 = \left[-\frac{1}{\Delta z}(\mathbf{C}_1 * \boldsymbol{\Omega}_2) + \frac{1}{2\Delta t}(\mathbf{C}_2 * \boldsymbol{\Omega}_2 - \mathbf{C}_3 * \boldsymbol{\Omega}_1) - \frac{\Delta x}{\Delta z \Delta t}(\mathbf{C}_1 * \boldsymbol{\Omega}_3) + \frac{\Delta x}{\Delta t^2}(\mathbf{C}_2 * \boldsymbol{\Omega}_3)\right]^{-1},$$

$$\mathbf{B}_2 = -\frac{1}{\Delta z}\mathbf{B}_1(\mathbf{C}_1 * \boldsymbol{\Omega}_2),$$

$$\mathbf{B}_3 = \frac{1}{2\Delta t}\mathbf{B}_1(\mathbf{C}_2 * \boldsymbol{\Omega}_2 - \mathbf{C}_3 * \boldsymbol{\Omega}_1),$$

$$\mathbf{B}_4 = -\frac{\Delta x}{\Delta z \Delta t}\mathbf{B}_1(\mathbf{C}_1 * \boldsymbol{\Omega}_3), \quad \mathbf{B}_5 = -\frac{\Delta x}{\Delta t^2}\mathbf{B}_1(\mathbf{C}_2 * \boldsymbol{\Omega}_3),$$

$$\mathbf{B}_6 = \frac{2}{\Delta x}\mathbf{B}_1(\mathbf{C}_3 * \boldsymbol{\Omega}_3). \tag{D-2}$$

Note that ζ is set to 1. For the migration problem ($\zeta = -1$), the expression should be solved for $\mathbf{U}_{j+\frac{1}{2}}^{k-1}$. Here, $\mathbf{U}_{j+1}$ is eliminated and equation 49 is rearranged to yield

$$\mathbf{U}_{j+\frac{1}{2}}^{k-1} = \mathbf{B}_2(-\mathbf{U}_{j+\frac{1}{2}}^{k+1} + \mathbf{U}_j^{k+1} + \mathbf{U}_j^{k-1}) + \mathbf{B}_3\mathbf{U}_{j+\frac{1}{2}}^{k+1} + \mathbf{B}_4(\mathbf{U}_{j+\frac{1}{2}}^{k+1} - \mathbf{U}_j^{k+1} + \mathbf{U}_j^{k-1}) + \mathbf{B}_5(\mathbf{U}_{j+\frac{1}{2}}^{k+1} - 2\mathbf{U}_{j+\frac{1}{2}}^{k}) + \mathbf{B}_6(\mathbf{U}_{j+\frac{1}{2}}^{k} - \mathbf{U}_{j+\frac{1}{2}}^{\prime k}), \tag{D-3}$$

where the coefficient matrices remain unchanged from equation D-2. It is possible to write a single expression for both the forward equation D-1 and migration equation D-3 solutions using a parameter γ, defined as

$$\gamma = \tfrac{1}{2}(1 + \zeta). \tag{D-4}$$

The general expression, by combining equations D-1 and D-3, can be written as

$$\mathbf{U}_{j+\frac{1}{2}}^{k+\zeta} = \mathbf{B}_2(-\mathbf{U}_{j+\frac{1}{2}}^{k-\zeta} + \mathbf{U}_{j+\gamma}^{k+1} + \mathbf{U}_{j+\gamma}^{k-1}) + \mathbf{B}_3\mathbf{U}_{j+\frac{1}{2}}^{k-\zeta} + \mathbf{B}_4(\mathbf{U}_{j+\frac{1}{2}}^{k-\zeta} + \zeta\mathbf{U}_{j+\gamma}^{k+1} - \zeta\mathbf{U}_{j+\gamma}^{k-1}) + \mathbf{B}_5(-2\mathbf{U}_{j+\frac{1}{2}}^{k} + \mathbf{U}_{j+\frac{1}{2}}^{k-1}) + \mathbf{B}_6(\mathbf{U}_{j+\frac{1}{2}}^{k} - \mathbf{U}_{j+\frac{1}{2}}^{\prime k}). \tag{D-5}$$

Note that the interior points are completely uncoupled and solved explicitly, while the boundary points are coupled with their associated auxiliary variables. This can be seen by observing that $\mathbf{B}_1$ is an inverse of a nondiagonal matrix (see equation D-2). However, since there are only a few auxiliary variables used at each boundary point, the size of $\mathbf{B}_1$ is small (usually less than five). Hence, the added computational effort is negligible.

REFERENCES

Asvadurov, S., V. Druskin, M. N. Guddati, and L. Knizhnerman, 2003, On optimal finite-difference approximation of PML: SIAM Journal on Numerical Analysis, **41**, 287–305.

Bamberger, A., B. Engquist, L. Halpern, and P. Joly, 1988, Higher-order paraxial wave-equation approximations in heterogeneous media: SIAM Journal on Applied Mathematics, **48**, 129–154.

Becker, E. B., G. F. Carey, and T. J. Oden, 1981, Finite elements — An introduction: Prentice-Hall, Inc.

Berenger, J. P., 1994, A perfectly matched layer for the absorption of electromagnetic waves: Journal of Computational Physics, **114**, 185–200.

Berkhout, A. J., 1985, Seismic imaging: Imaging of acoustic energy by wave field extrapolation, A: Theoretical aspects: Elsevier Science Publ. Co., Inc.

Brooke, G. H., and D. J. Thomson, 2000, Non-local boundary conditions for high-order parabolic equation algorithms: Wave Motion **31**, 117–129.

Chew, W. C., J. M. Jin, and E. Michielssen, 1997, Complex coordinate stretching as a generalized absorbing boundary: Microwave and Optical Technology Letters, 15, 363–369.

Claerbout, J. F., 1985, Imaging the earth's interior: Blackwell Scientific Publications, Inc.

Clayton, R. W., and B. Engquist, 1977, Absorbing boundary conditions for

acoustic and elastic wave equations: Bulletin of the Seismological Society of America, **6**, 1529–1540.
———, 1980, Absorbing boundary conditions for wave-equation migration: Geophysics, **45**, 895–904.
Collino, F., 1997, Perfectly matched absorbing layers for the paraxial equations: Journal of Computational Physics, **131**, 164–180.
Engquist, B., and A. Majda, 1977, Absorbing boundary conditions for numerical simulation of waves: Mathematics of Computation, **31**, 629–651.
———, 1979, Radiation boundary conditions for acoustic and elastic wave calculations: Communications on Pure and Applied Mathematics, **32**, 313–357.
Gardner, G. H. F., 1985, Migration of seismic data: SEG.
Givoli, D., 2004, High-order local non-reflecting boundary conditions: A review: Wave Motion, **39**, 319–326.
Guddati, M. N., 2006, Arbitrarily wide-angle wave equations for complex media: Computer Methods in Applied Mechanics and Engineering, **195**, 63–93.
Guddati, M. N., and A. H. Heidari, 2005, Migration with arbitrarily wide-angle wave equations: Geophysics, **70**, S61–S70.
Guddati, M. N., and K.-W. Lim, 2006, Continued fraction absorbing boundary conditions for convex polygonal domains: International Journal for Numerical Methods in Engineering, **66**, 949–977.
Howell, L. H., and L. N. Trefethen, 1988, Ill-posedness of absorbing boundary conditions for migration: Geophysics, **53**, 593–603.
Keys, R. G., 1985, Absorbing boundary conditions for acoustic media: Geophysics, **50**, 892–902.
Levy, M. F., 1997, Transparent boundary conditions for parabolic equation solution of radiowave propagation problems: IEEE Transactions on Antennas and Propagation, **45**, 66–72.
——–, 2001, Perfectly matched layer truncation for parabolic wave equation models: Proceedings of the Royal Society of London Series A-Mathematical Physics and Engineering Sciences, **457**, 2609–2624.
Lindman, E. L., 1975, Free-space boundary conditions for time-dependent wave equation: Journal of Computational Physics, **18**, 66–78.
Loewenthal, D., L. Lu, R. Robertson, and J. Sherwood, 1976, The wave equation applied to migration: Geophysical Prospecting, **24**, 380–399.
Papadakis, J. S., 1994, Exact, nonreflecting boundary conditions for parabolic-type approximations in underwater acoustics: Journal of Computational Acoustics, **2**, 83–98.
Raynolds, A. C., 1978, Boundary conditions for the numerical solution of wave propagation problems: Geophysics, **43**, 1099–1110.
Sacks, Z. S., O. M. Kingsland, R. Lee, and F. Lee, 1995, A perfectly matched anisotropic absorber for use as an absorbing boundary condition: IEEE Transactions on Antennas and Propagation, **43**, 1460–1463.
Shlager, K. L., and J. B. Schneider, 1995, Selective survey of the finite-difference time-domain literature: IEEE Antennas and Propagation Magazine, **37**, 39–57.
Stolt, R. H., and A. K. Benson, 1986, Seismic Migration: Geophysical Press.
Thomson, D. J., and M. E. Mayfield, 1994, An exact radiation condition for use with the *a posteriori* PE method: Journal of Computational Acoustics, **2**, 113–132.
Yevick, D., and D. J. Thomson, 1999, Nonlocal boundary conditions for finite-difference parabolic equation solvers: Journal of the Acoustical Society of America, **106**, 143–150.
——–, 2000, Impedance-matched absorbers for finite-difference parabolic equation algorithms: Journal of the Acoustical Society of America, **107**, 1226–1234.
Zhou, H. B., and G. A. McMechan, 2000, Rigorous absorbing boundary conditions for 3-D one-way wave extrapolation: Geophysics, **65**, 638–645.